AFRL-RX-WP-TP-2012-0234

MICROSTRUCTURE EVOLUTION AND COMPOSITION CONTROL DURING THE PROCESSING OF THIN-GAGE METALLIC FOIL (Preprint)

S.L. Semiatin and D.L. Ballard

Metals Branch
Metals, Ceramics, and NDE Division

M.E. Gross, D.W. Matson, W.D. Bennett, and C.D. Bonham

Pacific Northwest National Laboratory

A.I. Ustinov

E.O. Paton Electric Welding Institute

FEBRUARY 2012

AIR FORCE RESEARCH LABORATORY
MATERIALS AND MANUFACTURING DIRECTORATE
WRIGHT-PATTERSON AIR FORCE BASE, OH 45433-7750
AIR FORCE MATERIEL COMMAND
UNITED STATES AIR FORCE

REPORT DOCUMENTATION PAGE

Form Approved
OMB No. 0704-0188

1. REPORT DATE *(DD-MM-YY)*	2. REPORT TYPE	3. DATES COVERED *(From - To)*
February 2012	Journal Article Preprint	01 December 2011 – 01 December 2011

4. TITLE AND SUBTITLE

MICROSTRUCTURE EVOLUTION AND COMPOSITION CONTROL DURING THE PROCESSING OF THIN-GAGE METALLIC FOIL (Preprint)

5a. CONTRACT NUMBER
IN-HOUSE

5b. GRANT NUMBER

5c. PROGRAM ELEMENT NUMBER
62102F

6. AUTHOR(S)

S.L. Semiatin and D.L. Ballard (Metals, Ceramics, and NDE Division, Metals Branch (AFRL/RXLM))
M.E. Gross, D.W. Matson, W.D. Bennett, and C.D. Bonham (Pacific Northwest National Laboratory)
A.I. Ustinov (E.O. Paton Electric Welding Institute)

5d. PROJECT NUMBER
4347

5e. TASK NUMBER
20

5f. WORK UNIT NUMBER
25100102

7. PERFORMING ORGANIZATION NAME(S) AND ADDRESS(ES)

Metals, Ceramics, and NDE Division
Metals Branch (AFRL/RXLM)
Materials and Manufacturing Directorate, Air Force Research Laboratory
Wright-Patterson Air Force Base, OH 45433-7750
Air Force Materiel Command, United States Air Force

Pacific Northwest National Laboratory
E.O. Paton Electric Welding Institute

8. PERFORMING ORGANIZATION REPORT NUMBER
AFRL-RX-WP-TP-2012-0234

9. SPONSORING/MONITORING AGENCY NAME(S) AND ADDRESS(ES)

Air Force Research Laboratory
Materials and Manufacturing Directorate
Wright-Patterson Air Force Base, OH 45433-7750
Air Force Materiel Command
United States Air Force

10. SPONSORING/MONITORING AGENCY ACRONYM(S)
AFRL/RXLM

11. SPONSORING/MONITORING AGENCY REPORT NUMBER(S)
AFRL-RX-WP-TP-2012-0234

12. DISTRIBUTION/AVAILABILITY STATEMENT
Approved for public release; distribution unlimited.

13. SUPPLEMENTARY NOTES
PAO case number 88ABW-2011-6331, cleared 08 December 2011. The U.S. Government is joint author of this work and has the right to use, modify, reproduce, release, perform, display, or disclose the work. Submitted to Metallurgical and Materials Transactions A. Document contains color.

14. ABSTRACT

The manufacture of thin-gage superalloy and gamma-titanium-aluminide foil products via near-conventional thermomechanical processing (TMP) and two different vapor-deposition methods was investigated. TMP was based on hot-pack rolling of plate and sheet. Foils of the superalloy LSHR and the near-gamma titanium aluminide Ti-45.5Al-2Cr-2Nb made by this approach exhibited excellent gage control and fine two-phase microstructures. The vapor-phase techniques utilized magnetron sputtering (MS) of a target of the desired product composition or electron-beam physical vapor deposition (EBPVD) of separate targets of the specific alloying elements. Thin deposits of LSHR and Ti-48Al-2Cr-2Nb made by MS showed uniform thickness/composition and an ultrafine microstructure. However, systematic deviations from the specific target composition were found. During subsequent heat treatment, the microstructure of the MS samples showed various degrees of grain growth and coarsening. Foils of Ti-43Al and Ti-51Al-1V fabricated by EBPVD were fully dense.

15. SUBJECT TERMS
foil, thermomechanical processing, magnetron sputtering, electron-beam physical vapor deposition, superalloys, gamma-titanium-aluminide alloys

16. SECURITY CLASSIFICATION OF:			17. LIMITATION OF ABSTRACT:	18. NUMBER OF PAGES	19a. NAME OF RESPONSIBLE PERSON (Monitor)
a. REPORT	b. ABSTRACT	c. THIS PAGE			Donna Ballard
Unclassified	Unclassified	Unclassified	SAR	54	19b. TELEPHONE NUMBER *(Include Area Code)* N/A

MICROSTRUCTURE EVOLUTION AND COMPOSITION CONTROL DURING THE PROCESSING OF THIN-GAGE METALLIC FOIL

S.L. Semiatin, M.E. Gross*, D.W. Matson*, W.D. Bennett*, C.D. Bonham*, A.I. Ustinov**, and D.L. Ballard

Air Force Research Laboratory, Materials and Manufacturing Directorate, AFRL/RXLM, Wright-Patterson Air Force Base, OH 45433-7817, USA
* Pacific Northwest National Laboratory, Energy and Environment Directorate, Richland, WA 99352 USA
** E.O. Paton Electric Welding Institute, Kiev 03150, Ukraine

ABSTRACT

The manufacture of thin-gage superalloy and gamma-titanium-aluminide foil products via near-conventional thermomechanical processing (TMP) and two different vapor-deposition methods was investigated. TMP was based on hot-pack rolling of plate and sheet. Foils of the superalloy LSHR and the near-gamma titanium aluminide Ti-45.5Al-2Cr-2Nb made by this approach exhibited excellent gage control and fine two-phase microstructures. The vapor-phase techniques utilized magnetron sputtering (MS) of a target of the desired product composition or electron-beam physical vapor deposition (EBPVD) of separate targets of the specific alloying elements. Thin deposits of LSHR and Ti-48Al-2Cr-2Nb made by MS showed uniform thickness/composition and an ultrafine microstructure. However, systematic deviations from the specific target composition were found. During subsequent heat treatment, the microstructure of the MS samples showed various degrees of grain growth and coarsening. Foils of Ti-43Al and Ti-51Al-1V fabricated by EBPVD were fully dense. The microstructures developed during EBPVD were interpreted in terms of measured phase equilibria and the dependence of evaporant flux on temperature.

Key Words: Foil, thermomechanical processing, magnetron sputtering, electron-beam physical vapor deposition, superalloys, gamma-titanium-aluminide alloys.

I. INTRODUCTION

Honeycomb and truss-core products made from thin-gage sheet and foil are used for a variety of applications requiring characteristics such as light weight, high structural stiffness, or low thermal conductivity. Ductile, low temperature metals such as aluminum and low-carbon steel are readily produced in thin gages via ingot-metallurgy approaches consisting of successive hot- and cold-working operations to produce billet/bloom, plate, sheet, and foil with or without intermediate annealing steps. By contrast, the wrought manufacture of high-temperature, difficult-to-work materials such as nickel-base superalloys and intermetallic alloys can be substantially more challenging and costly due to a narrow processing window, the need for numerous intermediate anneals when using cold rolling to produce final gage, and low product yield. In extreme cases, such as the production of intermetallic gamma-titanium-aluminide foil, limited workability necessitates that all processing be done at hot-working temperatures via methods such as hot pack rolling [1, 2]. In turn, pack rolling of thin-gage products introduces stringent requirements related to pack design, can materials, and parting agents, each of which may affect reduction uniformity, surface finish, and thermal stress development/fracture during cool-down.

As an alternative to multi-step wrought processing, vapor-phase methods may enable the direct production of thin-gage foil. In this regard, two methods are promising, magnetron sputtering (MS) and electron-beam physical vapor deposition (EBPVD).

Magnetron sputtering (MS) yields relatively slow deposition rates of the order of 0.1 – 5 μm/h. It has been used at a laboratory scale to make small coupons of various gamma titanium aluminide alloys. For example, Abe, *et al.* [3], Banerjee, *et al.* [4], and

Senkov, *et al.* [5, 6] used magnetron sputtering onto *ambient-temperature* silicon or copper substrates to produce binary γ-TiAl or various quaternary and quinary alloys. The thickest samples (albeit of small plan-view area) were made by Senkov, *et al.* who produced free-standing foil using a polished, water-cooled copper substrate. In most cases, the sputtering process led to an essentially amorphous deposit, which can be ascribed to the use of the low-temperature substrate and hence the absence of measurable diffusion when titanium or solute atoms were deposited. The amorphous materials crystallized during post-sputtering heat treatment at temperatures of ~800-873K (~525-600°C). The phase(s) formed during crystallization varied in the different investigations, however. For example, Abe, *et al.* [3] noted a disordered hcp α solid solution and a new phase (ε) with a cubic crystal structure in the binary TiAl alloy. By contrast, the results of Banerjee, et al. [4] suggested that γ-TiAl can nucleate and grow directly from the amorphous matrix at least for a binary alloy. During continuous heating of Ti-46.5Al-2Nb-1.6Cr-0.5W (a/o), Senkov, *et al.* found that the crystallization sequence depended on the heating rate. At low heating rates (<20K/min), a metastable β phase formed initially and subsequently transformed into an hcp α structure which decomposed into a mixture of γ-TiAl and α_2 at temperatures above ~913K (~640°C). The formation of the intermediate β phase was suppressed at higher heating rates.

The importance of processing method, substrate temperature, and diffusional processes on deposit microstructure, albeit for a conventional titanium alloy, can be inferred at least qualitatively from the work of Warren and Wadley [7]. Although the specific processing conditions were not indicated, fully dense foils of Ti-6Al-4V (w/o)

measuring ~400 μm thick x 100 mm x 150 mm were produced using an argon-plasma sputtering technique and a *heated* stainless-steel substrate. The deposition rate was ~50 μm/h, or an order of magnitude faster than conventional magnetron sputtering; the thermal expansion mismatch between titanium and stainless steel led to a release of the foil from the substrate during system cool-down. In the as-deposited condition, the material exhibited a grain size between 30 and 100 nm and a high dislocation density. Heating to 1033K (760°C) led to the development of a coarser microstructure consisting of 500-nm-diameter alpha particles.

Typical deposition rates for the EBPVD process can be substantially higher compared to sputtering techniques. For EBPVD, the evaporation rate in terms of the flux J_s (in kg/m^{2}s) at the surface of the target is given by the Langmuir equation [8]:

$$J_s = X_i P_i^0 \Gamma_i (M_i / 2\pi R T)^{1/2} . \quad (1)$$

In this relation, X_i is the mole fraction of solute i, P_i^0 is the vapor pressure of pure element i at (absolute) temperature T, Γ_i is the activity coefficient of solute i in the liquid melt, M_i is the molar mass of solute i (in kg/mol), and R is the gas constant. For a target comprising a pure element, X_i =1 and Γ_i = 1. The Langmuir equation reveals that temperature dependence of the evaporation rate is controlled primarily by $P_i^0(T)$. For targets that comprise multi-component alloys, preferential evaporation of the high vapor-pressure alloying element(s), e.g., Al in a TiAl target, would be expected. Two approaches may be used to overcome such a difficulty: (1) the use of different targets at appropriate (different) surface melt temperatures or (2) the continuous feeding (and evaporation) of a bar with the desired composition under a steady-state condition [9].

The prediction of deposit microstructure during MS or EBPVD can be approached either phenomenologically or mechanistically. The phenomenological approach comprises the correlation of structure with process variables such as substrate temperature (MS or EBPVD) and sputtering-gas pressure (MS). For example, Movchan and Demchishin [10] and Thornton [11] developed processing diagrams which describe the evolution of voided vs dense columnar/equiaxed crystalline microstructures for a variety of pure elements and oxides. Hentzell, et al. [12] extended such approaches for thin films (thicknesses of the order of 100 nm). Per Movchan and Demchishin, the processing diagram for *EBPVD* deposits can be broken into three zones, the extent of each depending on deposition-substrate homologous temperature, T/T_m, in which T_m is the melting/liquidus temperature. The regions were denoted as zone 1 ($T/T_m < 0.3$, comprising a collection of discrete, tapered crystallites, separated by voids, with limited or no mechanical strength and whose width increases with substrate temperature), zone 2 ($0.3 < T/T_m < 0.5$, comprising columnar grains which still contain some porosity, but which have some strength and ductility), and zone 3 ($T/T_m > 0.6$, consisting of a columnar or equiaxed grain structure, depending on the specific deposited material, which is fully dense and as ductile as bulk material of the deposit composition). The qualitative difference in processing diagrams for thick *sputtered* deposits may be attributed to a variety of factors such as the kinetic energy of sputtered atoms, the approach of sputtered atoms from several directions, the presence of ambient gas, and bombardment of the substrate by the plasma [11]. Furthermore, it has been found that sputtered deposits tend to form fiber textures, typically <111> for fcc

metals and <110> for bcc metals, thus corresponding to close-packed planes lying in the plane of the deposit [11, 13].

From a mechanistic standpoint, microstructure evolution in vapor deposits depends on the typical kinetic factors of crystallite nucleation, grain-boundary migration, and possible recrystallization. Hence, boundary energy and mobility play key roles. Other factors, including the incident coating flux, the coating atom adsorption probability, the density of surface nucleation sites, and the surface mobility of adsorbed atoms, are also important. These factors depend on the substrate temperature, coating atom energy and angle of incidence, presence of foreign atoms, etc.

The objective of the current research was to assess the feasibility of using MS and EBPVD to make fully dense, thin-gage foil products of several difficult-to-work alloys. For this purpose, microstructures developed during deposition and subsequent heat treatment of a nickel-base superalloy and various gamma-titanium-aluminide alloys were evaluated and compared to baseline materials fabricated by near-conventional wrought (rolling) processes.

II. MATERIALS AND PROCEDURES

A. *Materials*

The materials for the present program consisted of (1) the powder-metallurgy (PM) superalloy LSHR (“low-solvus, high refractory”, an alloy developed originally by NASA for advanced disk applications [14]), (2) the two-phase (γ + α_2) near-gamma titanium aluminide alloys Ti-45.1Al-1.9Cr-1.9Nb and Ti-48.0Al-1.9Cr-2.1Nb (atomic percent), (3) nominally pure bars of titanium and aluminum, and (4) a Ti-V master alloy.

The LSHR superalloy was received as a 270-mm diameter billet produced by hot-isostatic pressing (HIP) of powder followed by hot extrusion to a 6:1 reduction. Its measured composition (in weight percent) was 20.4Co, 12.3Cr, 3.5Al, 3.5Ti, 2.7Mo, 4.3W, 1.5Nb, 1.5Ta, 0.045C, 0.027B, 0.05Zr, balance nickel. Its gamma-prime solvus temperature, $T_{\gamma'}$, above which ordered (L12) gamma-prime precipitates dissolve completely in the disordered (A1) fcc gamma matrix, was 1430K (1157°C).

The Ti-45.1Al-1.9Cr-1.9Nb material consisted of wrought 1-mm-thick sheet made by triple-arc melting of a 200-mm-diameter ingot, HIP, isothermal forging of cylindrical sections to a 6:1 reduction, and conventional hot pack rolling at 1533K (1260°C) to a 5:1 reduction of square performs extracted from the pancake forgings [2, 15]. The alpha-transus temperature of this material, T_{α} , above which $\alpha + \gamma \rightarrow \alpha$ (in which α denotes the disordered (A3) hcp phase, and γ is the ordered (L10) fct phase), was 1573K (1300°C). The ordering temperature, below which $\alpha \rightarrow \alpha_2$ (the ordered DO19 hexagonal, or Ti_3Al, phase), is 1398K (1125°C). The Ti-48.0Al-1.9Cr-2.1Nb alloy was received as a 200-mm diameter ingot which had been vacuum-arc melted and HIP'ed, but not wrought processed. Its alpha-transus temperature was approximately 1643K (1370°C).

B. *Experimental Procedures*

1. *Foil rolling*

Samples of both LSHR and Ti-45.1Al-1.9Cr-1.9Nb were hot pack rolled at the Air Force Research Laboratory using near-conventional practices to establish microstructure evolution and soundness of the finished product.

LSHR preforms measuring 63 x 63 x 11 mm were electric-discharge machined (EDM'ed) from the as-received extruded billet and encapsulated in cans of special design. Canned samples were hot-rolled at a speed of 125 mm/s on a two-high mill with 200-mm diameter x 300-mm wide rolls. Rolling comprised preheating (30 minutes) and reheating (2.5 minutes between each pass) in a furnace operated at 1378K ($T_{\gamma'}$ – 52K, or 1105°C). The reduction per pass was ~10 pct., and the total thickness reduction was 5.5:1. Following rolling, the workpiece was slow cooled in vermiculite and decanned. A section measuring 63 x 63 x 2.0 mm was EDM'ed from the rolled sheet, re-canned, hot rolled to foil with a thickness of 0.30 mm, and decanned using procedures similar to that employed for the prior sheet-rolling operation. Microstructures were determined using standard metallographic techniques for the as-rolled products as well as following a final one-hour heat treatment at 973, 1173, 1373, or 1473K (700, 900, 1100, or 1200°C); heat treatment was done on small samples encapsuled in quartz tubes which were evacuated and backfilled with argon. Backscattered electron (BSE) imaging was performed in a scanning electron microscope (SEM) equipped with a field-emission gun (FEG), viz., Sirion or Quanta 600F, both manufactured by FEI, Hillsboro, OR.

Foil processing of Ti-45.1Al-1.9Cr-1.9Nb was conducted in a similar fashion using the same equipment [2]. Specifically, performs measuring 75 x 75 x 0.8 mm were first annealed at 1523K (T_{α} - 50K, or 1250°C) for 2 h to spheroidize remnant lamellar colonies. They were then canned and rolled at 125 mm/s using a furnace preheat/reheat temperature of 1533K (1260°C) and reduction per pass of 12 pct. to a final foil thickness of ~0.2 mm. Microstructures were determined in the as-rolled condition as well as after a two-hour heat treatment at 1523K (1250°C).

2. *Magnetron sputtering*

The microstructures developed using the baseline wrought process were compared to those developed in thin samples of LSHR and Ti-48.0Al-1.9Cr-2.1Nb produced by unbalanced magnetron sputtering at the Pacific Northwest National Laboratory of the US Department of Energy. For each material, a 75 x 150 x 7.5 mm sputtering target was EDM'ed from the billet/ingot, stress relieved, finish ground, brazed onto an oxygen-free high-conductivity copper backing plate, and attached to an Angstrom Sciences Onyx 306 cathode. The cathode was mounted in a vacuum chamber having a stainless-steel shutter which enabled cleaning the surface of the sputtering target prior to initiating deposition (Figure 1a). Deposition substrates of nickel alloy 400 (with a nominal composition in weight percent of 31Cu, 2.5Fe max, 2.0 Mn max, 0.5 Si max, 0.3C max, balance nickel) were mounted on a rotatable heated holder which could be positioned over the ion source for substrate cleaning or over the cathode for deposition. A masked glass/sapphire witness sample was included on the substrate holder for each trial to obtain a step height measurement of the deposit thickness.

Each deposition trial was initiated by evacuating the chamber to a pressure of 6 x 10^{-7} Torr or better, introduction of the sputtering gas, and ion cleaning of the substrate by positioning it over the ion gun for 10 min. Sputtering was then performed in the DC mode using a current setting of 1 A and voltages ranging from ~350 to 600V. To obtain deposits with the highest possible integrity (i.e., minimum porosity), all experiments reported here utilized the maximum substrate-holder heater temperature (i.e., 973K, or 700°C). Furthermore, a substrate-deposit parting agent was not used to order to facilitate handling and metallography of the finished product. The principal process

parameters investigated were the target-substrate gap distance, the sputtering gas, gas pressure, and sputtering time/deposit thickness (Table I). The gap was varied between 75 mm (lower values tending to bring the substrate holder into the plasma confined at the cathode surface) and 125 mm (higher values leading to undesirably low deposition rates). The sputtering gas was argon, xenon, or krypton. Deposit thicknesses were between 5 and 50 μm.

As for the baseline wrought materials, the microstructures developed in the as-deposited condition or after identical heat treatments were determined via BSE imaging in a FEG-SEM.

3. *Electron-beam physical vapor deposition*

The third technique investigated to establish the broad feasibility of manufacturing thin-gage products was electron-beam physical vapor deposition (EBPVD). These trials focused on the fabrication of free-standing foils of the two-phase ($\gamma + \alpha_2$) alloy Ti-43Al and the single-phase (γ) alloy Ti-51Al-1V (atomic percent), and were conducted at the E.O. Paton Electric Welding Institute in Kiev, Ukraine.

The EBPVD set-up (Figure 1b) consisted of targets of pure Ti, pure Al, and Ti-V master alloy (used in various combinations), deposition substrates, and (not shown) the electron-beam (EB) guns used to melt/evaporate the targets. Because of the variation of evaporant flux with distance from the target, a partition (also shown in Figure 1b) was used in the system to “shadow” the vapor flow and thus enhance the ability to obtain uniform thickness and composition in deposits measuring 150 x 200 mm in plan area and ~150 μm in thickness. Held in water-cooled crucibles, the targets were located 300-mm under the substrates and were heated to pre-determined temperatures to control

the desired flux of each alloying element and hence the composition of the deposit. The substrates were a high-temperature alloy steel. They were heated to a temperature between 1123 and 1173K (850 and 900°C) using auxiliary EB guns and rotated at 30 rpm. Prior to deposition, a thin layer (~2-3 μm) of calcium fluoride, which served as a parting agent, was evaporated onto the substrates. Because of the large variation in the coefficient of thermal expansion of the foil deposit and the parting agent, the former separated readily during cooling following processing.

The microstructures of the EBPVD foils in the as-deposited condition or following a 2 h heat treatment at 1273K (1000°C) or 1423K (1150°C) were determined via BSE imaging in the FEG-SEM. Heat treatments for longer times or higher temperatures led to an extremely coarse microstructure or cavitation within the foil.

III. RESULTS AND DISCUSSION

The principal results from this investigation comprised observations and interpretations of foil integrity, composition, microstructure, and (in selected instances) crystallographic texture. To elucidate the effect of processing method on such factors, the results for the PM superalloy LSHR and the gamma titanium aluminide alloys are presented and discussed separately.

A. *LSHR*

1. *Wrought LSHR*

Sheet and foil of the PM superalloy LSHR were readily produced by near-conventional hot pack rolling (Figure 2). In the as-rolled condition, the only defects comprised limited edge cracking in the foil product (Figure 2b). The microstructures following rolling were somewhat finer (average grain size ~ 1-2 μm) compared to that in

the preform material preheated at the rolling temperature (average grain size ~ 2.5 μm) (Figure 3). However, the as-rolled microstructures for both the sheet and foil (Figures 3b, c) were only partially recrystallized. The lack of recrystallization can be attributed to the high volume fraction of gamma-prime precipitate at the rolling temperature (i.e., ~20 pct. at 1378K, or 1105°C) and thus the pinning effect of second-phase particles.

Heat treatment following rolling of the LSHR foil gave rise to varying degrees of recrystallization and grain growth (Figure 4). After heat treatment at either 973 or 1173K (700 or 900°C), the gamma grains appeared to have undergone little recrystallization and to have retained a moderate degree of elongation parallel to the rolling direction (Figures 4a, b). The (gray) gamma-prime particles, comprising ~50 pct. of the microstructure at these temperatures, were similarly elongated and unspheroidized. By contrast, heat treatment at the higher temperature of 1373K (1100°C, ~ the rolling temperature) led to partial gamma-grain recrystallization and partial spheroidization of the gamma-prime particles (Figure 4c). The complete dissolution of the gamma-prime pinning phase at 1473K ($T_{\gamma'}$ +47K, or 1200°C) resulted in full recrystallization and a noticeable amount of microstructural coarsening, thus yielding an average grain size of ~15 μm (Figure 4d). Limited solely by the presence of somewhat randomly-distributed carbides and borides (white particles in BSE images), this grain size was comparable to that observed previously for unrolled material heat treated at supersolvus temperatures [16]. The samples heat treated at the higher temperatures also showed a few isolated pores whose source is most likely residual argon gas from the powder atomization process.

2. *Magnetron-sputtered LSHR*

Thin LSHR samples fabricated by magnetron sputtering showed excellent thickness uniformity (Figure 5a), an absence of porosity, uniform composition, and fine microstructure. Furthermore, all of the LSHR deposits were completely bonded to the substrate (Figure 5a). The latter observations can be attributed to the absence of a parting agent and the similarity of the coefficients of thermal expansion of LSHR and the nickel alloy 400 substrate material, which would minimize differential contraction during cooling from 973K (700°C) following sputtering.

The uniformity of composition, as determined by wavelength dispersive spectroscopy (WDS), is illustrated in Figure 6 for sample 1-D-S, whose processing parameters are summarized in Table I. The longer-wavelength variations in the composition of each alloying element were typically of the order of $\pm$0.1 weight percent, or values of the same order of magnitude as the errors in the experimental measurements themselves; the superimposed variations of shorter wavelength (~2-4 μm) may be due to slight non-uniformity in the local volume fractions of gamma and gamma prime. Despite the relatively good chemical uniformity, there were systematic differences between the deposit and target compositions per se (Table II). Deviations from the target composition tended to be on the low side for aluminum, tantalum, and tungsten and on the high side for chromium and cobalt. The use of krypton or xenon sputtering gas (instead of argon) and a small cathode-substrate gap tended to reduce the aluminum deficiency substantially and the chromium excess partially (samples 1-I-M, 1-J-M, and 1-L-M in Tables I and II). However, these same process modifications tended to increase the negative deviations for the two heaviest alloying elements in

LSHR, i.e., tantalum and tungsten. Despite these differences, the reproducibility of the results suggests that a modified target composition can give a desired final product composition.

Magnetron sputtering produced crystalline deposits of LSHR as indicated by typical 111 and 100 fcc peaks in x-ray-diffraction data (not shown). The microstructure was extremely fine, consisting of grains elongated in the normal/deposition direction with an aspect ratio of ~5:1 (Figure 5b). The observed fully-dense structure of columnar-like grains can be rationalized on the basis of sputter-processing diagrams [11] which indicate such microstructures for $T_{substrate}/T_m$ ~ 0.6 and gas pressures of ~1- 3 mTorr, i.e., the conditions used in the present work. A relatively weak fiber-like texture (~2 x random) with <111> poles parallel to the sheet-normal (deposition) direction was found by electron backscatter diffraction (EBSD) analysis (Figures 7a, b); this texture is similar to that observed in the past for magnetron sputtered fcc metals of comparable thickness [11]. Similar textures were also observed in samples that were heat treated at various temperatures following deposition (Figures 7c-f).

The effect of post-sputtering heat-treatment temperature on the deposit microstructure (Figure 8) was qualitatively similar to that observed for rolled LSHR foil described in Section III.A.1. For example, after a 1 h heat treatment at 973 or 1173K (700 or 900°C) (Figures 8a, b), the microstructure was essentially unchanged, as was found for the rolled foil heat-treated at these temperatures (Figures 3c and 4a, b). The grains were still very fine and elongated as in the as-deposited condition (Figure 5b). After heat treatment at 1373K (1100°C) for 1 h, the structure appeared to be partially spheroidized with a mixture of equiaxed and elongated gamma grains (Figure 8c). The

grain boundaries were pinned by carbide/boride particles (imaging white in Figure 8c). The very fine gamma-prime precipitates likely produced during magnetron sputtering appeared not to have coarsened enough to be resolved by SEM BSE, but likely played a role in pinning of the grain boundaries at 1373K (1100°C) as well.

After heat treatment of the magnetron-sputtered LSHR above the gamma-prime solvus, i.e. at 1473K (1200°C), the grain structure was mostly equiaxed with a few remnant elongated grains (Figures 8 d, e). The grain size was ~5 μm, which was smaller than that produced during the identical supersolvus heat treatment of rolled LSHR foil, i.e., ~15 μm (Figure 4d). Two factors appear to have contributed to the finer grain size in the magnetron-sputtered material. First, the carbide/boride particles were nucleated and hence located preferentially at the grain boundaries in the sputtered material, unlike the more random particle arrangement in the corresponding foil product. Second, because the sputtered deposit was very thin (50 μm), a large fraction of the grains had boundaries adjacent to the free surface or the deposition substrate (Figure 8e). The free surface would have provided a pinning force [17], and reaction with the substrate could have limited the diffusional processes that control grain growth.

B. *Gamma Titanium-Aluminide Alloys*

The results for the various near-gamma (γ + α_2) and single-phase γ titanium aluminide alloys are discussed in the context of the phase equilibria summarized in Figure 9. All compositions cited below are in atomic percent.

1. *Wrought Ti-45.5Al-2Cr-2Nb*

Rolled foil of the two-phase (γ + α_2) Ti-45.5Al-2Cr-2Nb alloy (Figure 10a) exhibited good gage control and fine microstructure. The final thickness of the various

foils was in the range of 200-250 μm. Furthermore, the thickness of a given foil was fairly uniform with a maximum variation of approximately ±15 μm relative to the mean (Figure 10b).

The as-rolled microstructures (Figures 10b, c) were typical of those for $\gamma + \alpha_2$ near-gamma titanium-aluminide alloys. They comprised fine primary γ particles (darker phase in BSE images) in a matrix of fine $\gamma + \alpha_2$ lamellae; at the rolling temperature, the matrix was single-phase (disordered) α (Figure 9a). Because the material contains two phases whose volume fractions are comparable to each other, possible variations in the overall composition of the rolled products could not be readily ascertained via WDS. However, the similarity of the volume fractions of the primary γ and matrix phases at all locations served as an indirect indicator of the good composition uniformity. In this regard, reference to the pseudo-binary phase diagram for Ti-xAl-2Cr-2Nb (Figure 9a) reveals that a one atomic percent variation in aluminum would give rise to a 20 pct. variation in the volume fraction of γ particles at 1533K (1260°C).

The microstructure of the rolled foil following a 2 h heat treatment at 1523K (1250°C) was also relatively fine and uniform (Figure 10d). Heat treatment tended to fully spheroidize those γ particles which had exhibited a small amount of elongation. The larger α_2 grains (light grains in BSE images) appeared featureless. This appearance was due to the rapid cooling rate experienced by very thin foil samples when extracted from the heat-treatment furnace and allowed to air cool. Such rapid cooling rates would suppress the decomposition of the high-temperature α phase and result in a matrix of α_2 grains or very fine $\gamma + \alpha_2$ lamellae which could not be resolved in SEM images. In

contrast, the slow cooling imparted to prevent thermal shock following rolling of large canned samples allowed ample time for the $\alpha \rightarrow \gamma + \alpha_2$ reaction within the matrix to form the observed lamellar microstructures seen in Figures 10b, c.

2. *Magnetron-sputtered Ti-48Al-2Cr-2Nb*

Metallographic examination of magnetron-sputtered gamma titanium-aluminide samples indicated that uniform composition could be obtained, but microstructure control may require a somewhat higher substrate temperature than was possible with the present equipment.

WDS composition traverses parallel and perpendicular to the deposition direction revealed uniform composition with little scatter. However, there was a measurable dependence of composition on the specific set of processing parameters. The most noticeable variation was the aluminum content which was close to that of the target for sample γ-G, but approximately 2 atomic percent higher in samples γ-J and γ-K (Table III). Both of the latter two samples had been fabricated using krypton sputtering gas rather than argon which was utilized for the other two specimens (Table I). The WDS results also indicated small variations in chromium and niobium composition relative to that of the target, the former being slightly higher and the latter slightly lower. These deviations were systematic and could thus be readily be corrected by choice of a target with slightly different chemistry.

The microstructures of the as-sputtered materials were similar to each other (Figure 11). Each comprised fibrous/columnar grains with very thin gaps between them. The length of the gaps tended to be less in samples γ-J and γ-K produced with the (heavier) Xe gas, an observation analogous to previous findings for magnetron-

sputtered tantalum [20]. The present microstructures can be rationalized on the basis of magnetron-sputtering processing maps [11]. Such phenomenological correlations suggest that processing conditions comprising a sputtering gas pressure of ~3 mTorr and $T_{substrate}/T_m$ = 0.55 =(973/1773), as used in the present work, lie very close to the boundary between microstructures consisting of densely packed fibrous grains and fully dense columnar grains extending through the thickness of the deposit.

The microstructure of magnetron-sputtered samples of the γ-TiAl underwent noticeable changes during subsequent heat treatment (Figure 12). During heat treatment at 1273K (1000°C), the fine, lenticular porosity between the fibrous grains was eliminated or coalesced into pores with a diameter of ~ 1 μm (Figures 12a, b). The microstructures following heat treatment at this temperature also mirrored the small difference in aluminum content among the various samples. Specifically, sample γ-G (with 48.5 a/o Al) showed a two-phase phase (γ + α_2) microstructure, whereas samples γ-H, J, K (with 49.5-50.5 a/o Al) comprised single-phase γ grains. These observations are in agreement with trends suggested by the binary Ti-Al phase diagram (Figure 9b).

The bottom 35-50 pct. of each sample heat treated at 1273K (1000°C) also revealed evidence of reaction with the nickel alloy 400 substrate (e.g., Figure 12). The reaction was confirmed by WDS which showed substantial diffusion of copper and nickel from the substrate into the deposit. Heat treatment at 1423K (1150°C) essentially destroyed the entire layer of γ + α_2 or γ due to what appeared to be the formation of a Ti-Ni-X-type eutectic between alloying elements in the deposit and the substrate. These results strongly suggest the need to develop a parting agent which is suitable for

separating the foil from the substrate immediately following fabrication, thereby avoiding chemical interactions during final heat treatment.

3. *EBPVD single-phase-gamma titanium-aluminide foils*

Large-plan-area foils (~150 mm x 200 mm) of the single-phase gamma and near-gamma titanium-aluminide alloys (e.g., Figure 13) were free of porosity, but showed a thickness variation of ~±10 pct. relative to the average. Moreover, following the initial set-up trials, it was determined that the maximum peak-to-peak variation in aluminum content across the thickness of a given foil could be reliably controlled to ~2 to 4 atomic percent.

Optical micrographs for the nominally single-phase alloy Ti-51Al-1V showed some non-uniformity in microstructure (Figure 14a). It consisted of separate regions of equiaxed γ grains and what appeared to be a lamellar phase. Several possible sources may be hypothesized to explain this observation - composition variations or an effect associated with the specific processing parameters. With regard to the first possibility, aluminum variations across the thickness of this foil in the as-fabricated condition were approximately 2 atomic percent, i.e., from ~50 to 52 atomic percent (Figure 15a). Assuming a minimal effect of small levels of vanadium on phase equilibria,, the Ti-Al phase diagram (Figure 9b) suggests that such variations would be insufficient to change the microstructure from one which is single-phase γ to one which is two-phase ($\gamma + \alpha_2$) . This conclusion was supported by BSE images (not shown) which indicated that the microstructure was indeed single-phase γ.

Concerning the second possibility, the ratio of the temperature of the deposition substrate (~1123-1173K, or ~850-900°C) to the liquidus temperature of Ti-51Al

(~1743K, or 1470°C) would yield a value of T/T_m of approximately 0.65. The EBPVD processing diagrams for various materials [10] indicate a transition at T/T_m at ~0.6 from a so-called zone 2 microstructure (columnar grains which still contain some porosity) to a zone 3 microstructure (a fully dense material with columnar or equiaxed grains). The observation of the mixed microstructure in the present work may thus be inferred to have resulted from processing conditions lying close to the transition region. More specifically, such temperatures lie in a regime in which bulk diffusion and recrystallization begin to become likely. Such phenomena would be more likely for the bottom regions of the foil (i.e., those deposited first during the multi-hour process used in the present work) and less likely for the layers deposited last. As a result, the bottom layers of the foil would be expected to comprise equiaxed grains and the upper layers would be columnar in nature, as was observed (Figure 14a).

Because EBPVD occurred close to conditions which typically give rise to microstructural transitions, a small variation in substrate temperature during processing could also have contributed to the microstructural heterogeneity noted in the as-deposited condition.

Following heat treatment at 1273K (1000°C), the microstructure of the Ti-51Al-1V EBPVD foil was fully equiaxed (Figure 14b), comprising coarse or fine γ grains in the regions that had been either lamellar or equiaxed, respectively, in the as-deposited condition. Heat treatment at 1423K (1150°C) produced a much coarser structure of equiaxed γ grains, although differences in grain size on the two sides of the foil were still noticed (Figure 14c). The 2 h heat treatment at the higher temperature also tended to reduce the composition variation slightly (Figures 15a vs 15b).

Process controls required to minimize composition variations during EBPVD of gamma titanium-aluminide foil products from individual elemental targets was evaluated using the Langmuir equation (Equation (1)) for the specific case of evaporation of a *pure* element as a function of temperature, i.e.,

$$J = P_o\,(M/\,2\pi R\,T)^{1/2}\,. \qquad (2)$$

Here, M denotes the molar mass (in kg/mol), T is the absolute temperature, R is the gas constant, and P_o is the vapor pressure of the element as a function of temperature per the Clausius-Clapeyron equation, i.e.,

$$P_o\,[\mathrm{Pa}] = 133\;10^{(-A/T+B)}\,T^{C} \qquad (3)$$

in which A, B, and C are material constants. For liquid Al, A = 16379, B = 9.98, and C = -0.335; for liquid Ti, A = 22946, B = 10.58 and C = -0.373 [21].

The effect of small variations in EBPVD target/melt-pool temperature on the flux J can be readily quantified by examining the variational form of Equation (1) after taking the common logarithm of both sides and noting that $\log_{10}X = (1/2.303)\,\ln_e X$:

$$(\delta J)/J = [(\delta T)/T] \times [(2.303A/T) + C - 0.5]. \qquad (4)$$

As an example, the evaporation of separate titanium and aluminum targets to produce the equiatomic (Ti-50Al) composition is considered; in weight percent, this composition corresponds to Ti-36Al. Thus the fluxes (in kg/m^2s) should be in the ratio of $J_{Al}:J_{Ti}$ = 36:64. If the aluminum target is maintained at nominally 1500K (1227°C), the titanium target should be heated to ~2055K (1782°C) to obtain the appropriate flux ratio. Using Equation (4), a 3K (3C°) variation in target/melt-pool temperature during evaporation would give a fractional variation in flux of ~5 percent for aluminum at 1500K (1227°C) and ~4 percent for Ti at 2055K (1782°C), thus producing variations of the order of 2 –

2.5 atomic percent for each alloying element. The present results suggest that the temperature transients may indeed have been of this order for the fabrication of the Ti-51Al-1V foil. For other single-phase gamma titanium-aluminide alloys, such temperature variations may be acceptable unless one target experiences a hotter temperature of this magnitude and the other a slightly cooler temperature.

4. *EBPVD near-gamma titanium-aluminide foils*

Optical and SEM backscatter-electron photographs of the microstructures developed in foil of the two-phase (γ + α_2) titanium aluminide alloy Ti-43Al highlighted challenges when composition is not carefully controlled within a narrow range for materials of this type. In particular, the optical microstructure (Figure 16a) was noticeably finer than in the wrought product (Figure 10c) except for a band of coarse grains near the midplane of the foil. During subsequent heat treatment, both the fine and coarse-grain regions underwent some growth (Figures 16b, c). The extent of microstructure coarsening was either somewhat limited or quite noticeable during heat treatment at 1273K (1000°C) or 1423K (1150°C), respectively.

The source of non-uniform microstructure in the Ti-43Al foils was deduced from BSE micrographs (Figure 16d, e, f) in which the darker phase is γ and the lighter phase is α_2. These micrographs revealed that the volume fractions of γ and α_2 were not totally uniform and that bands of coarser γ grains were produced in areas with lower amounts of α_2. A general coarsening of both phases during heat treatment following EBPVD was also revealed by the BSE micrographs.

The magnitude of the composition transients during processing that would give rise to the microstructure observations for the EBPVD Ti-43Al samples was ascertained

by reference to the Ti-Al phase diagram (Figure 9b). Under equilibrium conditions, the γ:α_2 phase ratio at 1273K (1000°C) would be ~50:50 for Ti-43Al. On the other hand, this ratio would be ~25:75 for Ti-40Al or 75:25 for Ti-46Al. Hence, the relative narrow α_2 + γ phase field for two-phase near-gamma titanium aluminide alloys mandates close control of the flux of the constituent alloying elements during EBPVD.

IV. SUMMARY AND CONCLUSIONS

Microstructure evolution and composition control during magnetron sputtering (MS) and electron-beam physical vapor deposition (EBPVD) of thin-gage materials were established for several superalloy and gamma titanium aluminide alloys. Based on this research, the following conclusions have been drawn:

1. Although (baseline) wrought processing of foil by hot pack rolling is costly, such near-conventional methods produce uniform, fine microstructures with good control of gage.

2. MS gives rise to very fine, uniform microstructures in multi-component superalloys such as LSHR in both the as-fabricated and deposited-and-heat-treated conditions. The microstructures developed in LSHR by this means are finer than those in the wrought baseline material. Systematic differences in composition between the target and deposit can be mitigated through selection of specific target composition, sputtering gas, and sputtering variables.

3. MS can also be used to obtain desired, uniform composition in thin-gage gamma-titanium-aluminide products through proper specification of target composition. However, a relatively high deposition substrate temperature and a suitable parting agent

must be utilized to control microstructure and avoid contamination during final heat treatment.

4. EBPVD offers significant potential for economic production of large-plan-area foils of single- and two-phase gamma titanium aluminide alloys with a microstructural scale comparable to or significantly finer than in the corresponding wrought material. However, EBPVD processing using elemental materials to make multi-component alloys in this class requires very close control of target temperatures and evaporant fluxes.

Acknowledgements – This work was conducted as part of the in-house research of the Metals Branch of the Air Force Research Laboratory's Materials and Manufacturing Directorate. The support and encouragement of the Laboratory management and, in particular, the Air Force Office of Scientific Research (Drs. Joan Fuller and A. Sayir, program managers) are gratefully acknowledged. The assistance of M.A. Guisfredi, T.T. Gorman, and W.M. Saurber in sample characterization is appreciated. Portions of this work were conducted under the auspices of a MIPR with Pacific Northwest National Laboratory (PNNL), which is operated by Battelle Memorial Institute for the U.S. Department of Energy under Contract DE-AC06-76RLO1830, and AFOSR/EOARD Partner Project P-339 with Paton Institute, which was awarded through the Science and Technology Center of Ukraine (STCU).

REFERENCES

1. S.L. Semiatin: *Gamma Titanium Aluminides,* Y-W. Kim, R. Wagner, and M. Yamaguchi, eds., TMS, Warrendale, Pennsylvania, 1995, pp. 509-24.
2. S.L. Semiatin, B.W. Shanahan, and F. Meisenkothen: *Acta Mater.*, 2010, vol. 58, pp. 4446-4457.
3. E. Abe, M Ohnuma, and M. Nakamura: *Acta Mater.*, 1999, vol. 47, pp. 3607-3616.
4. R. Banerjee, S. Swaminathan, R. Wheeler, and H.L. Fraser: *Phil. Mag. A*, 2000, vol. 80, pp. 1715-1727.
5. O.N. Senkov, M.D. Uchic, S. Menon, and D.B. Miracle: *Scripta Mater.*, 2002, vol. 46, pp. 187-192.
6. O.N. Senkov and M.D. Uchic: *Mater. Sci. Eng. A*, 2003, vol. A340, pp. 216-224.

7. J. Warren and H.N.G. Wadley: *Aerospace Thermal Structures and Materials for a New Era*, E.A. Thornton, ed., American Institute of Aeronautics and Astronautics, Reston, VA, 1995, pp. 323-342.
8. I. Langmuir: *Phys. Rev.*, 1913, vol. 5, pp. 329-342.
9. R.J. Hill: *Physical Vapor Deposition*, Temescal Division of BOC Group, Berkeley, CA, 1986.
10. B. A. Movchan and A.V. Demchishin: *Fiz. Metal. Metalloved.*, 1969, vol. 28, pp. 653-660.
11. J.A. Thornton: *J. Vac. Sci. Techn.*, 1974, vol. 11, pp. 666-670.
12. H.T.G. Hentzell, C.R.M. Grovenor, and D.A. Smith: *J. Vac. Sci. Techn. A*, 1984, vol. A2, pp. 218-219.
13. D.B. Knorr, D.P. Tracy, and K.P. Rodbell: *Defect Structure, Properties, and Morphology of Deposits*, H. Merchant, ed., TMS, Warrendale, PA, 1995, pp. 323-333.
14. T. P. Gabb, J. Gayda, J. Telesman, P. T. Kantzos, and W. A. Konkel: Report NASA/TM-2003-212086, National Aeronautics and Space Administration, Glenn Research Center, Cleveland, OH, Jan 2003.
15. S.L. Semiatin and V. Seetharaman: *Metall. Mater. Trans. A*, 1995, vol. 26A, pp. 371-381.
16. S.L. Semiatin, K. E. McClary, A.D. Rollett, C.G. Roberts, E.J. Payton, F. Zhang, and T.P. Gabb: *Metall. Mater. Trans. A*, 2011, in press.
17. Y. Wang: Unpublished research, the Ohio State University, Columbus, OH, 2003.
18. S.L. Semiatin, V. Seetharaman, and V.K. Jain: *Metall. Mater. Trans. A*, 1994, vol. 25A, pp. 2753-2768.
19. C. McCullough, J.J. Valencia, C.G. Levi, and R. Mehrabian: *Acta Metall.*, 1989, vol. 37, pp. 1321-1336.
20. D.W Matson, E.D McClanahan, J.P Rice, S.L Lee, and D. Windover: *Surface and Coatings Technology*, 2000, vols. 133-134, pp. 411-416.
21. A.I. Efimov, L.P. Belorukova, I.V. Vasil'kova, and V.P. Chechev: *Properties of Inorganic Compounds*, Chimiya, Leningrad, 1983, pp. 298-313. (in Russian)

Table I. Process Parameters for Magnetron-Sputtering Trials

Material	ID	Gap (mm)	Gas	Pressure (mTorr)
LSHR	1-D-S	105	Ar	3
LSHR	1-A-M	75	Ar	3
LSHR	1-D-M	125	Ar	3
LSHR	1-E-M	125	Ar	2.1
LSHR	1-F-M	105	Ar	2.2
LSHR	1-I-M	75	Kr	2.4
LSHR	1-J-M	75	Xe	2.5
LSHR	1-L-M	75	Xe	1
TiAl*	γ-G	75	Ar	5
TiAl*	γ-H	75	Ar	2.7
TiAl*	γ-J	75	Kr	2.6
TiAl*	γ-K	75	Kr	1.6

* TiAl = Ti-48.0Al-1.9Cr-2.1Nb

Table II. WDS Composition Measurements (Weight Percent) for Magnetron-Sputtered LSHR Samples

ID	Al	Ti	Cr	Co	Nb	Mo	Ta	W	Ni
1-D-S	2.57	3.29	14.6	23.3	1.41	2.89	1.35	4.02	Bal.
1-A-M	2.52	3.30	13.8	22.7	1.38	2.77	1.29	3.98	Bal.
1-D-M	2.57	3.28	14.4	23.0	1.38	2.82	1.26	3.92	Bal.
1-E-M	2.51	3.25	14.5	23.1	1.4	2.86	1.27	3.97	Bal.
1-F-M	2.44	3.28	14.2	22.8	1.4	2.86	1.36	4.03	Bal.
1-I-M	3.15	3.30	13.4	22.5	1.34	2.67	1.23	3.6	Bal.
1-J-M	3.28	3.28	13.5	22.4	1.39	2.77	1.3	3.78	Bal.
1-L-M	3.2	3.26	13.9	22.7	1.37	2.74	1.27	3.65	Bal.
Target	3.42	3.50	12.6	21.3	1.48	2.69	1.54	4.32	Bal.
Target*	3.49	3.48	12.3	20.4	1.51	2.72	1.59	4.24	Bal.

* Mill certification/wet chemical analysis

Table III. WDS Composition Measurements (Atomic Percent) for As-Magnetron-Sputtered Gamma Titanium Aluminide Samples

ID	Al	Cr	Nb	Ti
γ-G	48.5±0.17	2.28±0.02	1.62±0.03	Bal.
γ-H	49.4±0.17	2.27±0.02	1.57±0.03	Bal.
γ-J	50.4±0.20	2.27±0.02	1.45±0.03	Bal.
γ-K	50.3±0.11	2.28±0.01	1.46±0.02	Bal.
Target*	48.0	1.90	2.10	Bal.

* Mill certification/wet chemical analysis

Figure Captions

Figure 1. Illustrations of equipment used in the present investigation for (a) magnetron sputtering and (b) electron-beam physical vapor deposition (EBPVD).

Figure 2. Macrographs of LSHR produced by near-conventional hot pack rolling: (a) Sheet and (b) foil.

Figure 3. BSE images of the grain structures developed in LSHR during processing at 1378K ($T_{\gamma'}$ -52K, or 1105°C): (a) Undeformed/heat treated alone, (b) as-rolled sheet, and (c) as-rolled foil. The small particles within the gamma grains in (a) are gamma-prime precipitates. The rolling direction is horizontal and the normal direction is vertical in (b) and (c).

Figure 4. BSE images of the grain structures developed in LSHR foil during post-rolling heat treatment for 1 h at (a) 973K (700°C), (b) 1173K (900°C), (c) 1373K (1100°C), or (d) 1473K (1200°C). The gray particles in (a)-(c) are gamma prime; the white particles are carbides and borides.

Figure 5. BSE images of as-deposited magnetron-sputtered LSHR sample 1-D-S (Table I) photographed at (a) low or (b) high magnification.

Figure 6. Composition profiles taken across magnetron-sputtered LSHR sample 1-D-S.

Figure 7. EBSD data for magnetron-sputtered LSHR sample 1-D-S: (a) Normal-(deposition-) direction inverse-pole-figure map and (b) 111 pole figure for as-deposited condition, and 111 pole figures after a 1 h heat treatment at (c) 973K (700°C), (d) 1173K (900°C), (e) 1373K (1100°C), or (f) 1473K (1200°C). The center of each pole figure corresponds to the normal direction.

Figure 8. BSE images of the microstructures developed in magnetron-sputtered LSHR sample 1-D-S during heat treatment for 1 h at (a) 973K (700°C), (b) 1173K (900°C), (c) 1373K (1100°C), or (d, e) 1473K (1200°C).

Figure 9. Phase equilibria of importance for titanium-aluminide program alloys: (a) Partial pseudo-binary phase diagram for Ti-xAl-2Cr-2Nb [18] and (b) binary phase diagram for Ti-Al [19].

Figure 10. Rolled foil of Ti-45.5Al-2Cr-2Nb (atomic percent): (a) Macrograph of de-canned foil, (b, c) BSE micrographs of as-rolled foil at two different magnifications, and (d) BSE micrograph of rolled foil after a 2 h heat treatment at 1523K (1250°C). In (b, c, d), the rolling direction is horizontal and thickness direction vertical. The white layer on the top and bottom surfaces of the foil in (b) is nickel plating.

Figure 11. BSE images of as-deposited magnetron-sputtered samples of Ti-48Al-1.9Cr-2.1Nb: (a, b) γ-G, (c) γ-H, and (d) γ-K. The processing conditions are given in Table I.

Figure 12. BSE images of the microstructures developed during heat treatment at 1273K (1000°C) in magnetron-sputtered TiAl samples (a) γ-G and (b) γ-K. (Note that the deposit in (a) separated from its substrate during cool-down following heat treatment.)

Figure 13. Macrograph of as-fabricated 150-μm thick EBPVD foil of Ti-51Al-1V (atomic percent).

Figure 14. Polarized light optical photographs of the microstructure in EBPVD foils of Ti-51Al-1V (atomic percent) in (a) the as-fabricated condition or following a 2 h heat treatment at (b) 1273K (1000°C) or (c) 1423K (1150°C).

Figure 15. Aluminum composition profiles taken across EBPVD foil samples of Ti-51Al-1V (atomic percent) in (a) the as-fabricated condition or (b) following a subsequent 2 h heat treatment at 1423K (1150°C).

Figure 16. Microstructures in EBPVD foil of Ti-43Al (atomic percent) in (a, d) the as-deposited condition or following a following a 2 h heat treatment at (b, e) 1273K (1000°C) or (c, f) 1423K (1150°C); (a, b, c) polarized light, optical-microscopy images or (d, e, f) backscatter-electron images.

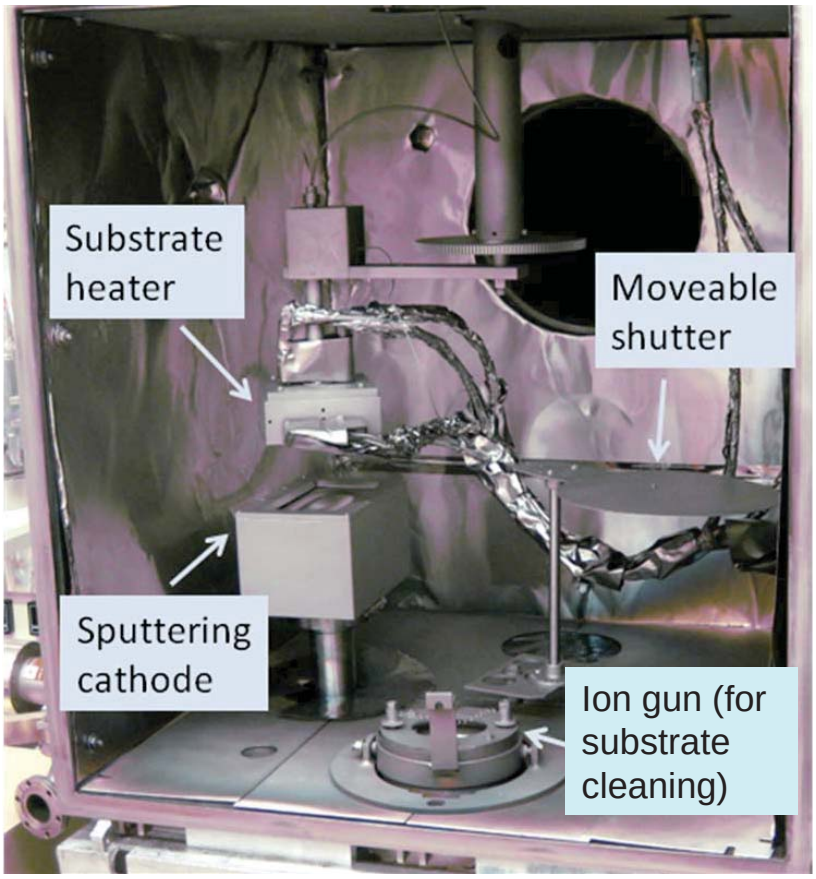

(a)

Figure 1. Illustrations of equipment used in the present investigation for (a) magnetron sputtering and (b) electron-beam physical vapor deposition (EBPVD).

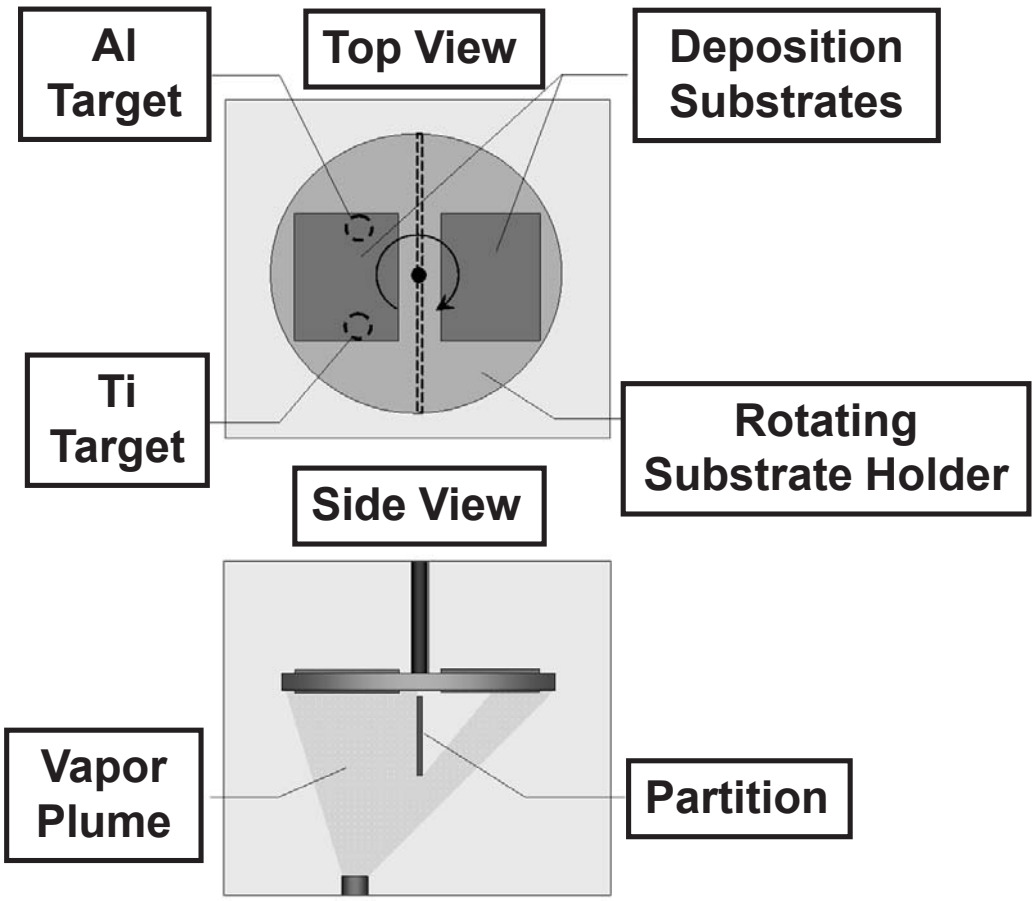

(b)

Figure 1. (Cont'd)

Figure 2. Macrographs of LSHR produced by near-conventional hot pack rolling: (a) Sheet and (b) foil.

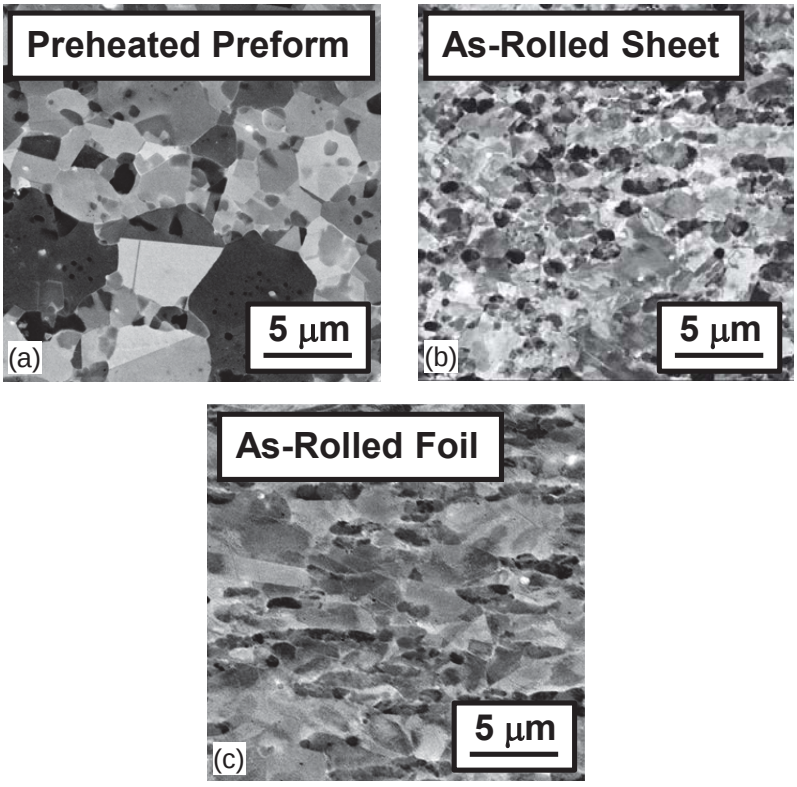

Figure 3. BSE images of the grain structures developed in LSHR during processing at 1378K ($T_{\gamma'}$ -52K, or 1105°C): (a) Undeformed/heat treated alone, (b) as-rolled sheet, and (c) as-rolled foil. The small particles within the gamma grains in (a) are gamma-prime precipitates. The rolling direction is horizontal and the normal direction is vertical in (b) and (c).

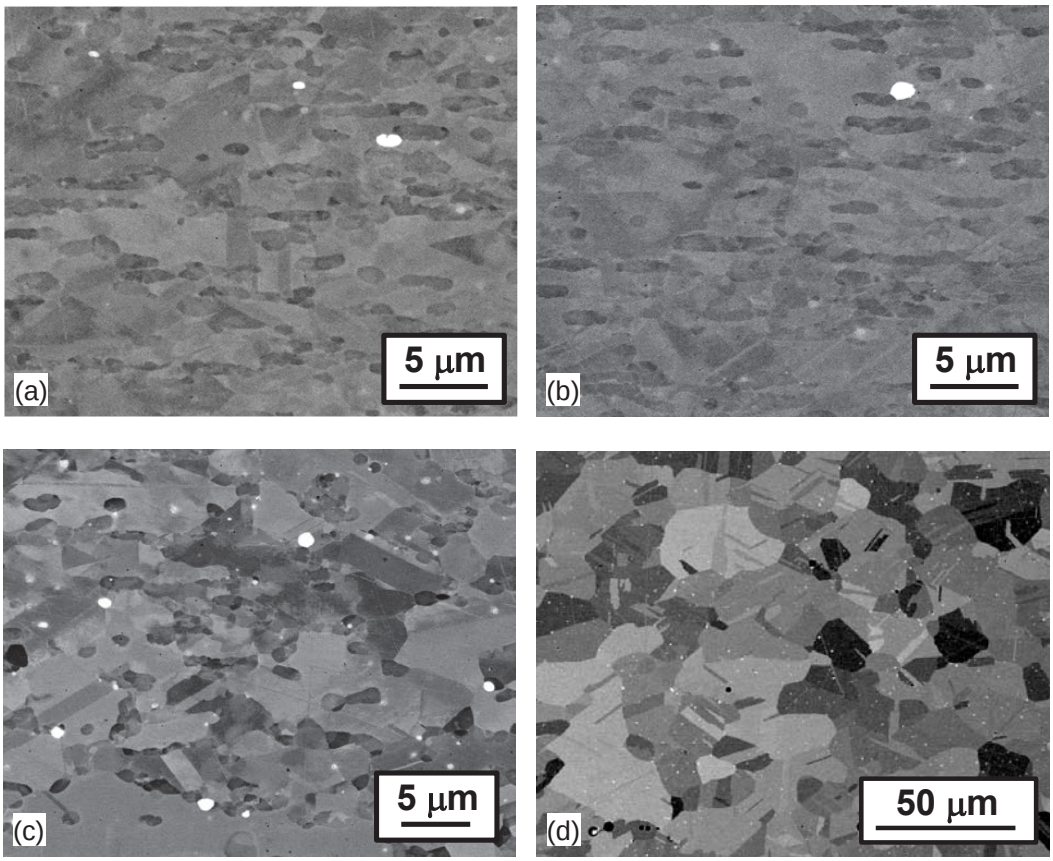

Figure 4. BSE images of the grain structures developed in LSHR foil during post-rolling heat treatment for 1 h at (a) 973K (700°C), (b) 1173K (900°C), (c) 1373K (1100°C), or (d) 1473K (1200°C). The gray particles in (a)-(c) are gamma prime; the white particles are carbides and borides.

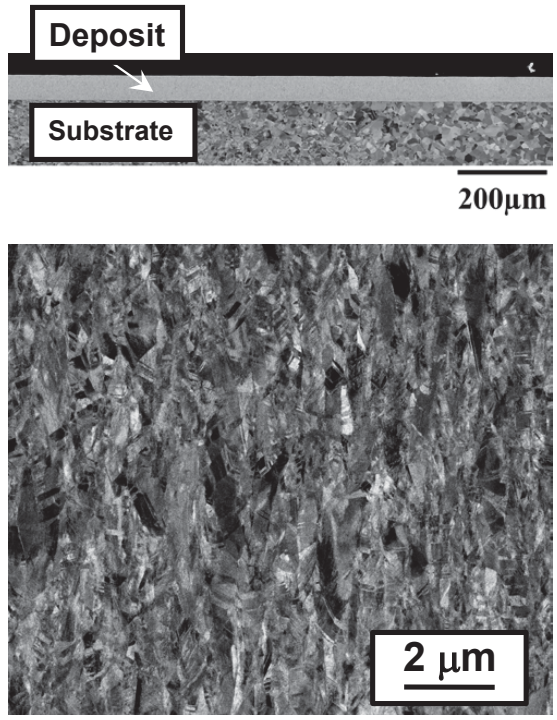

Figure 5. BSE images of as-deposited magnetron-sputtered LSHR sample 1-D-S (Table I) photographed at (a) low or (b) high magnification.

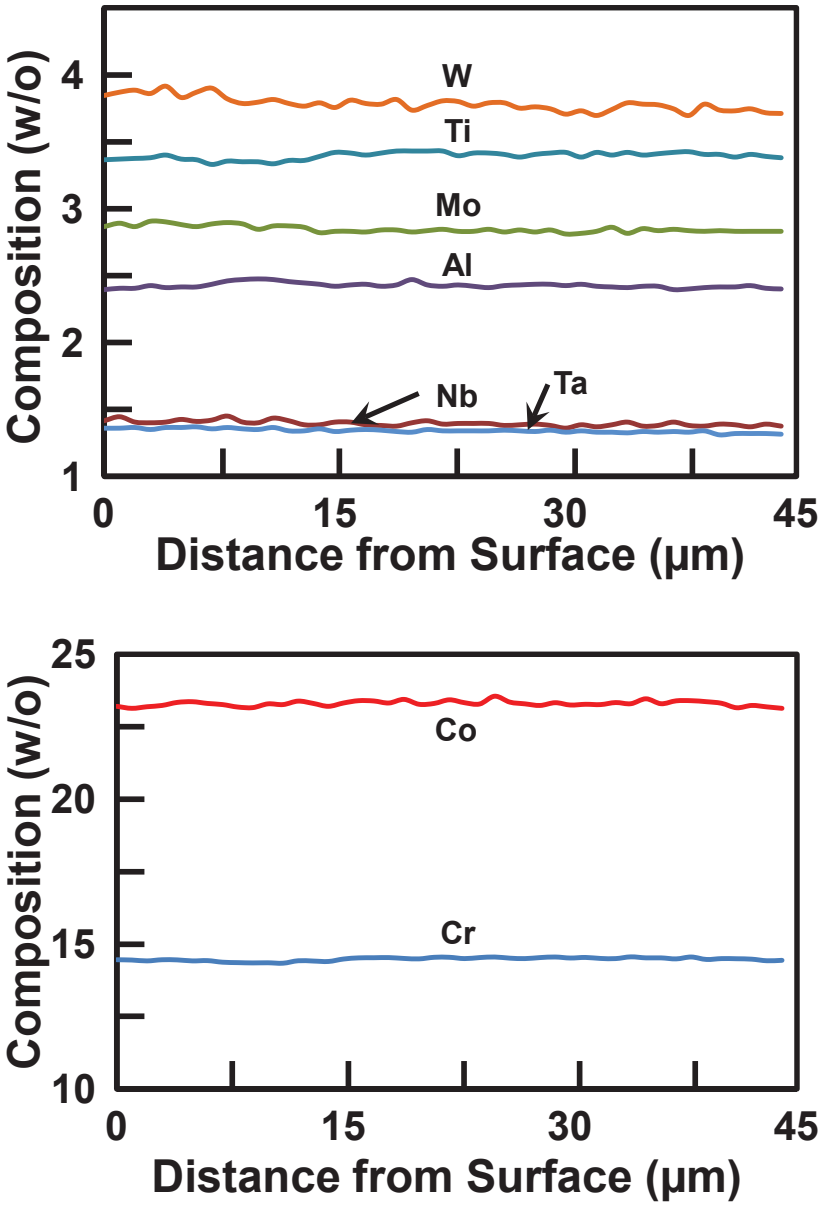

Figure 6. Composition profiles taken across magnetron-sputtered LSHR sample 1-D-S.

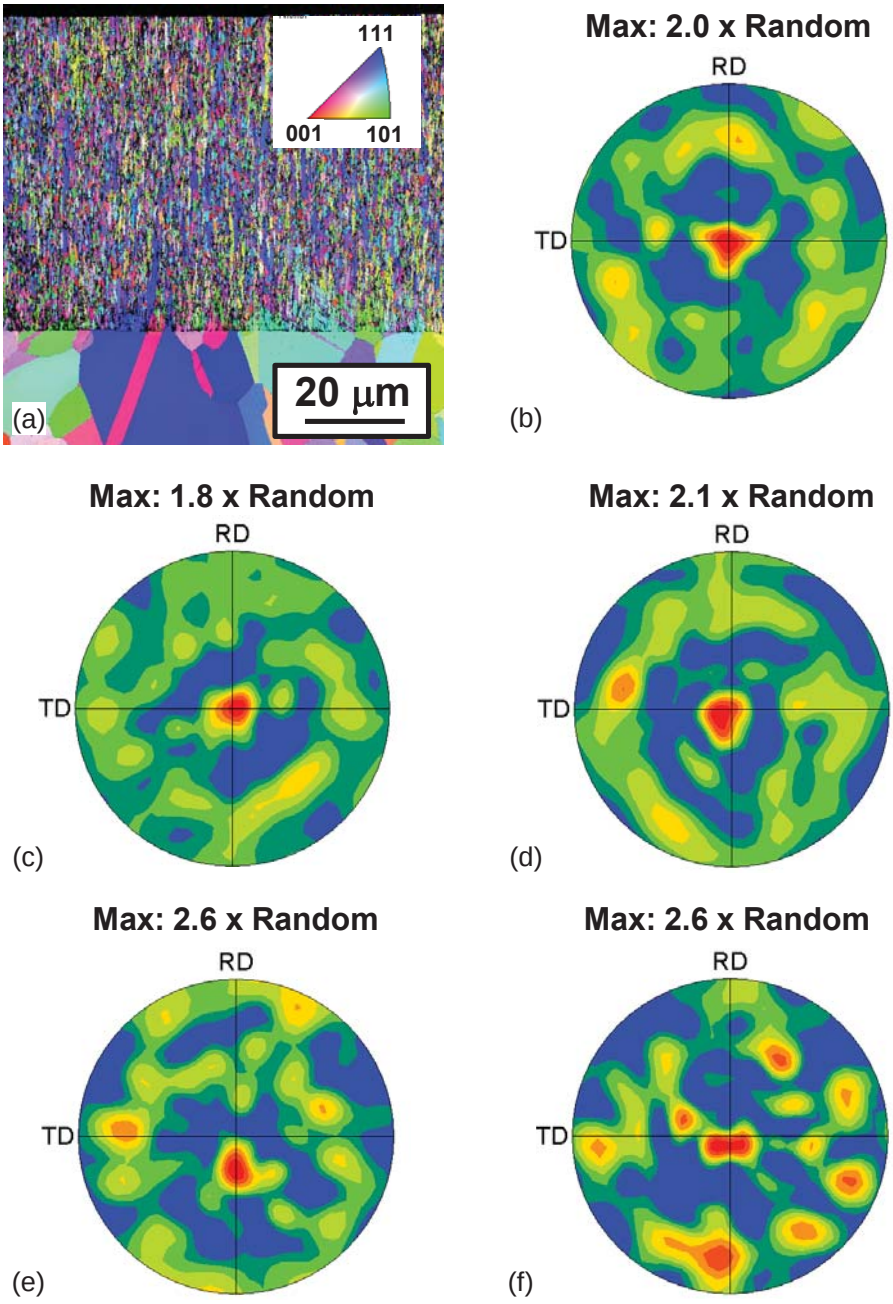

Figure 7. EBSD data for magnetron-sputtered LSHR sample 1-D-S: (a) Normal-(deposition-) direction inverse-pole-figure map and (b) 111 pole figure for as-deposited condition, and 111 pole figures after a 1 h heat treatment at (c) 973K (700°C), (d) 1173K (900°C), (e) 1373K (1100°C), or (f) 1473K (1200°C). The center of each pole figure corresponds to the normal direction.

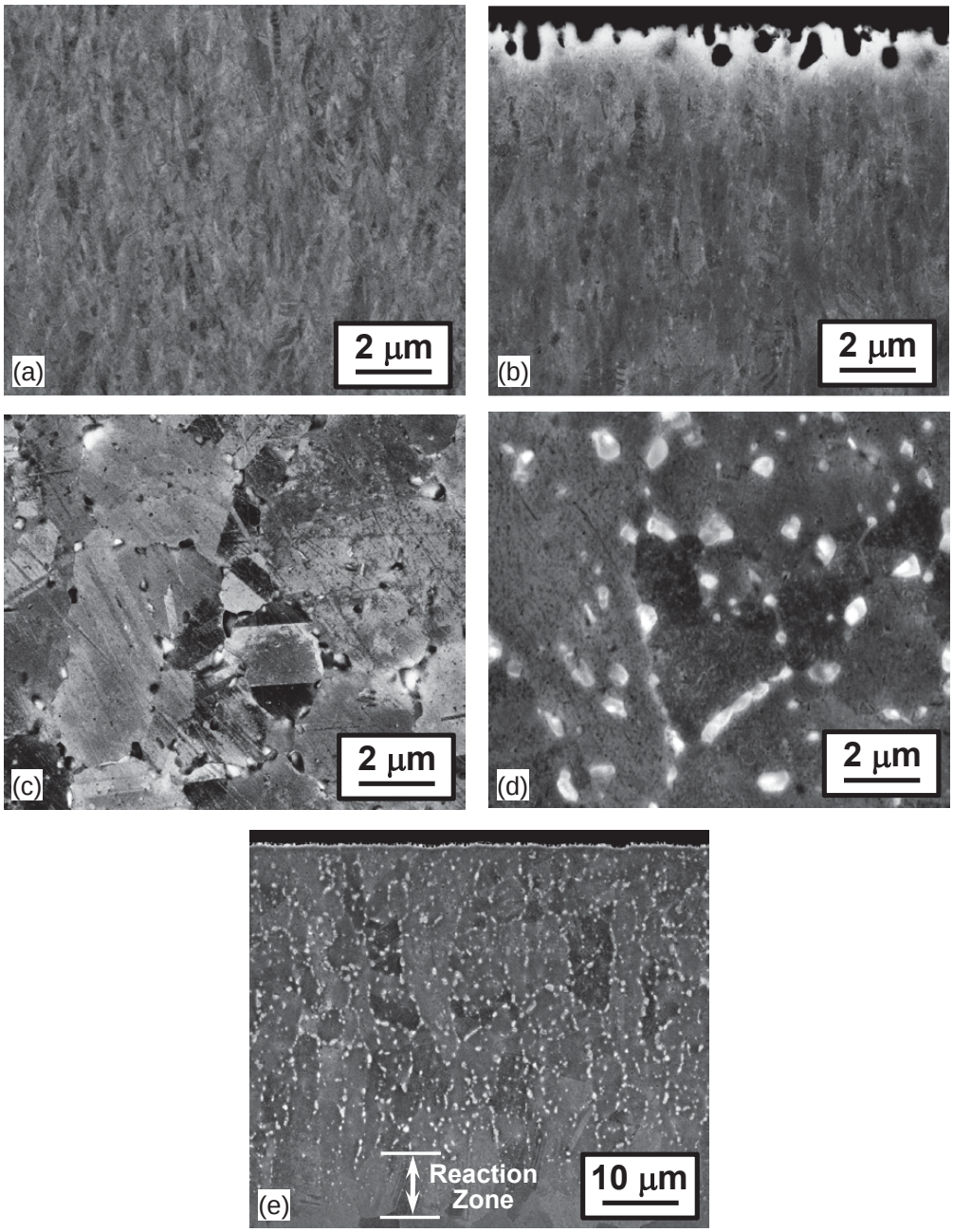

Figure 8. BSE images of the microstructures developed in magnetron-sputtered LSHR sample 1-D-S during heat treatment for 1 h at (a) 973K (700°C), (b) 1173K (900°C), (c) 1373K (1100°C), or (d, e) 1473K (1200°C).

(a)

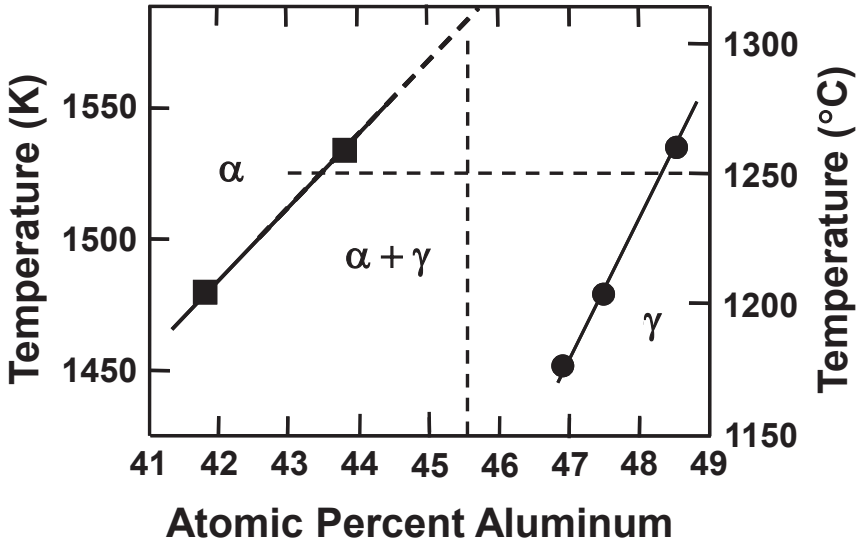

(b)

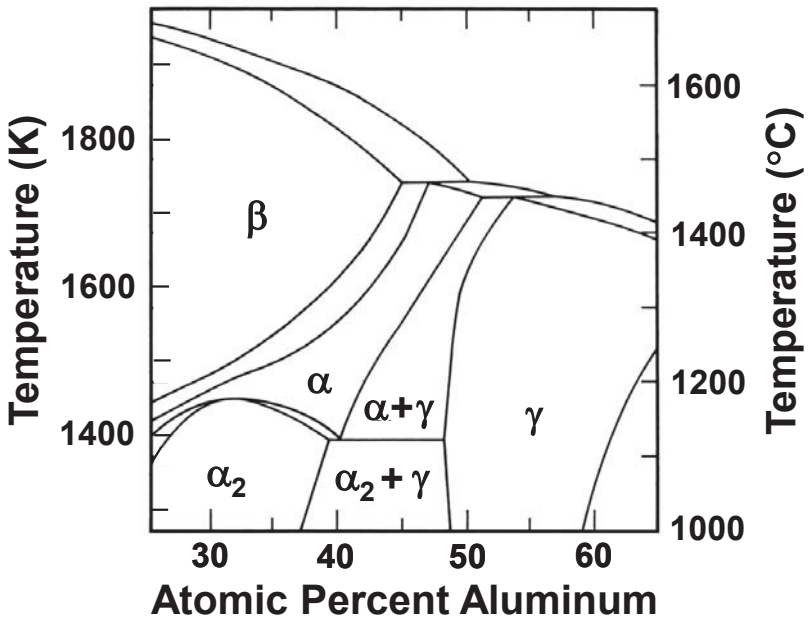

Figure 9. Phase equilibria of importance for titanium-aluminide program alloys: (a) Partial pseudo-binary phase diagram for Ti-xAl-2Cr-2Nb [18] and (b) binary phase diagram for Ti-Al [19].

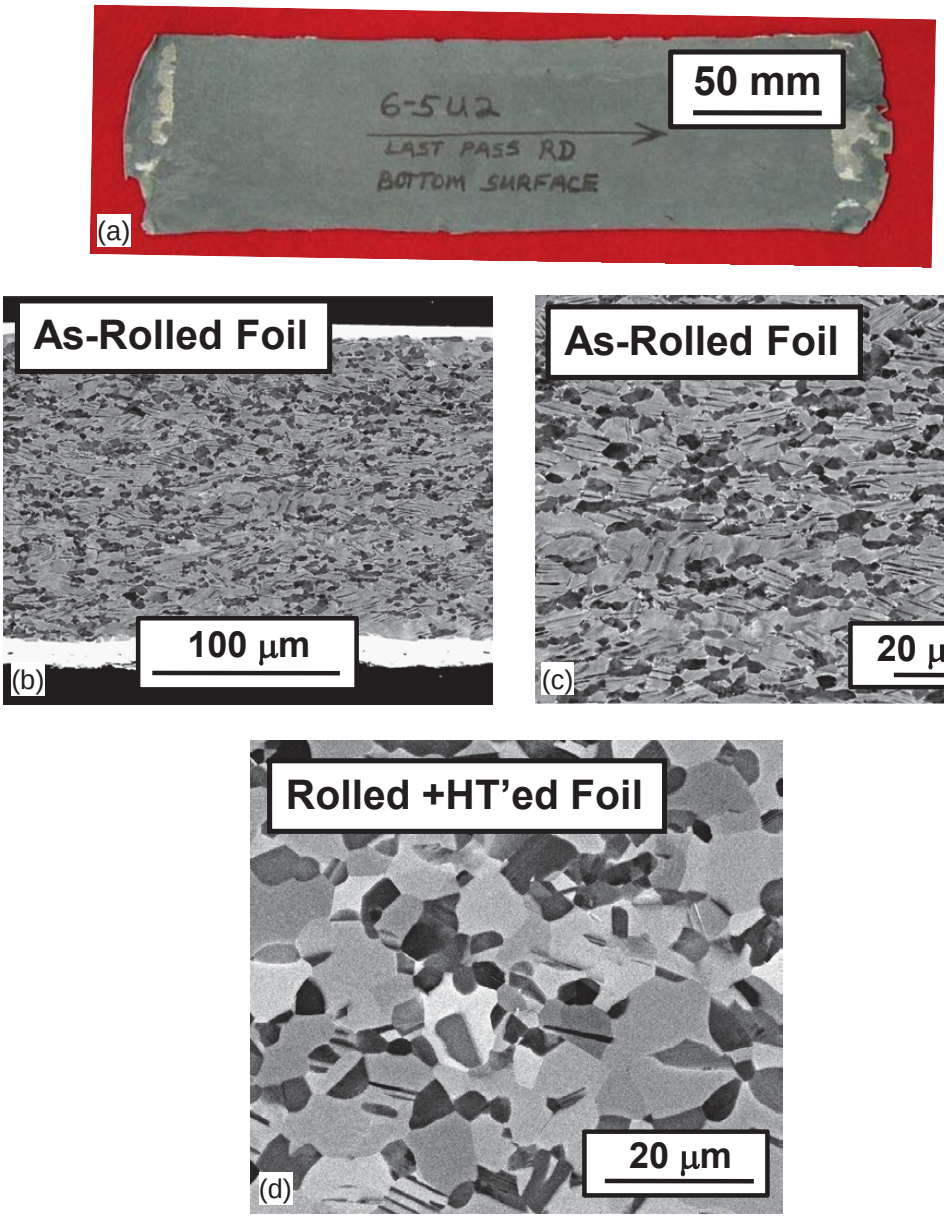

Figure 10. Rolled foil of Ti-45.5Al-2Cr-2Nb (atomic percent): (a) Macrograph of de-canned foil, (b, c) BSE micrographs of as-rolled foil at two different magnifications, and (d) BSE micrograph of rolled foil after a 2 h heat treatment at 1523K (1250°C). In (b, c, d), the rolling direction is horizontal and thickness direction vertical. The white layer on the top and bottom surfaces of the foil in (b) is nickel plating.

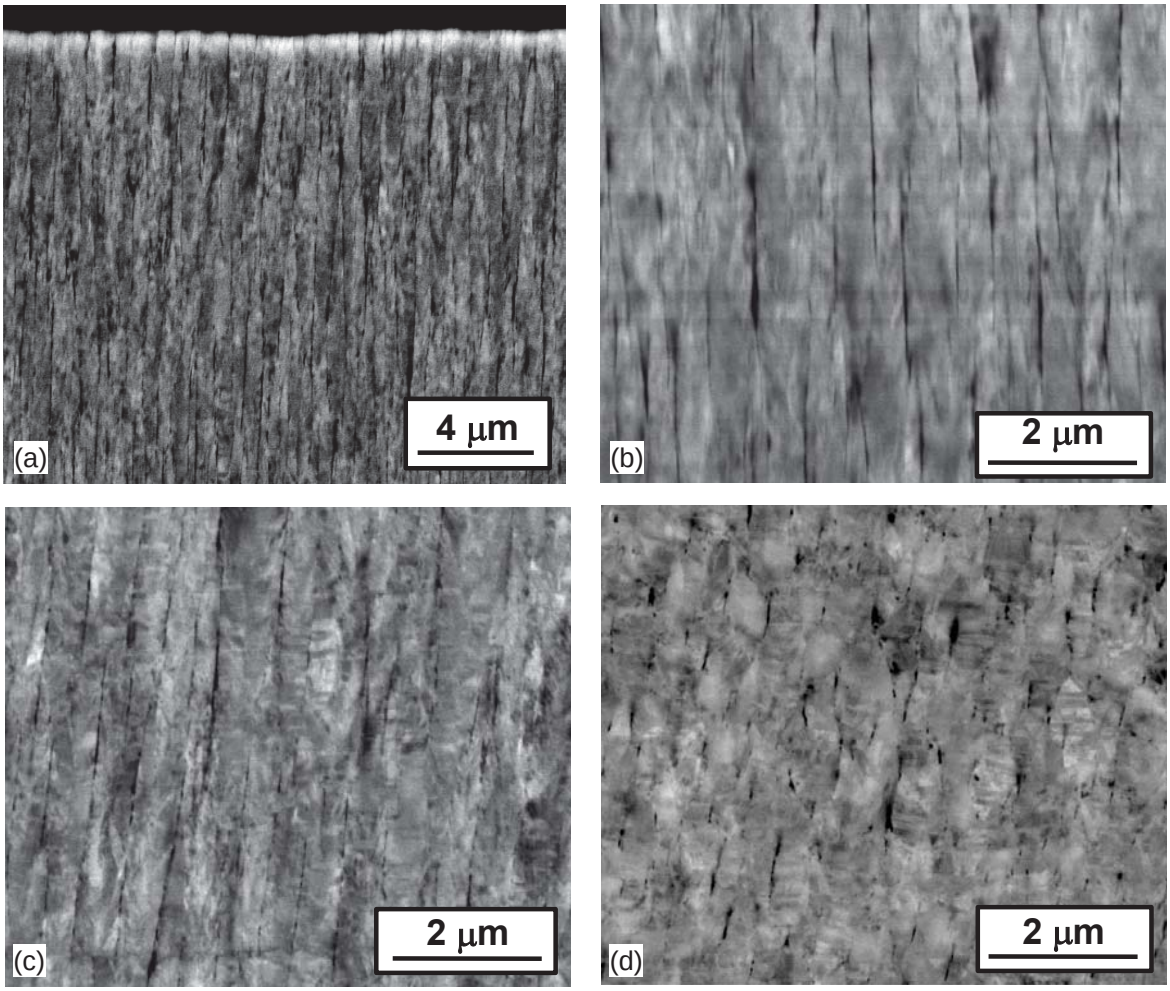

Figure 11. BSE images of as-deposited magnetron-sputtered samples of Ti-48Al-1.9Cr-2.1Nb: (a, b) γ-G, (c) γ-H, and (d) γ-K. The processing conditions are given in Table I.

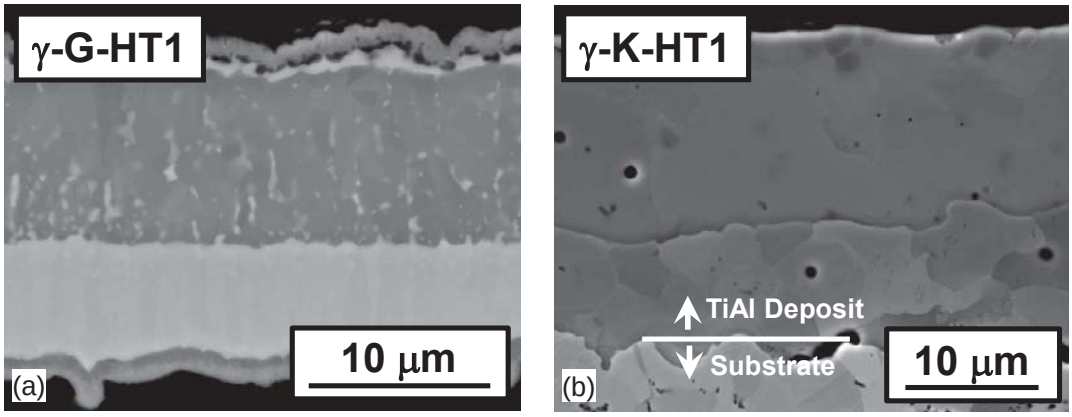

Figure 12. BSE images of the microstructures developed during heat treatment at 1273K (1000°C) in magnetron-sputtered TiAl samples (a) γ-G and (b) γ-K. (Note that the deposit in (a) separated from its substrate during cool-down following heat treatment.)

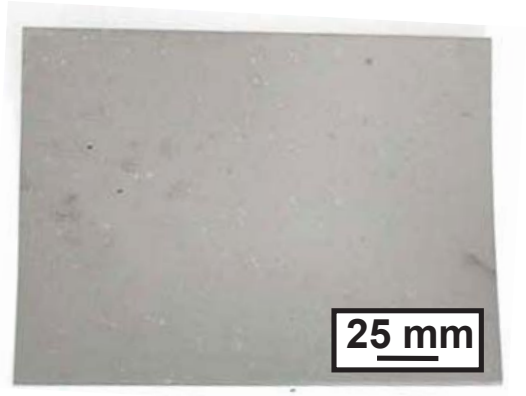

Figure 13. Macrograph of as-fabricated 150-μm thick EBPVD foil of Ti-51Al-1V (atomic percent).

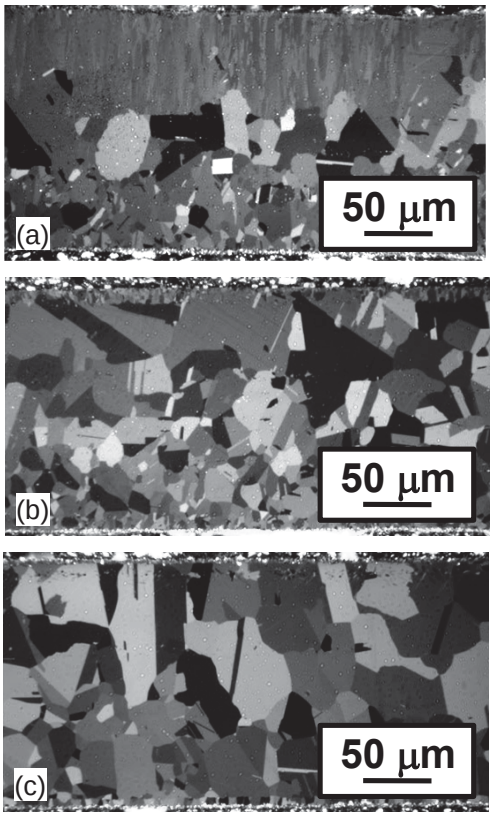

Figure 14. Polarized light optical photographs of the microstructure in EBPVD foils of Ti-51Al-1V (atomic percent) in (a) the as-fabricated condition or following a 2 h heat treatment at (b) 1273K (1000°C) or (c) 1423K (1150°C).

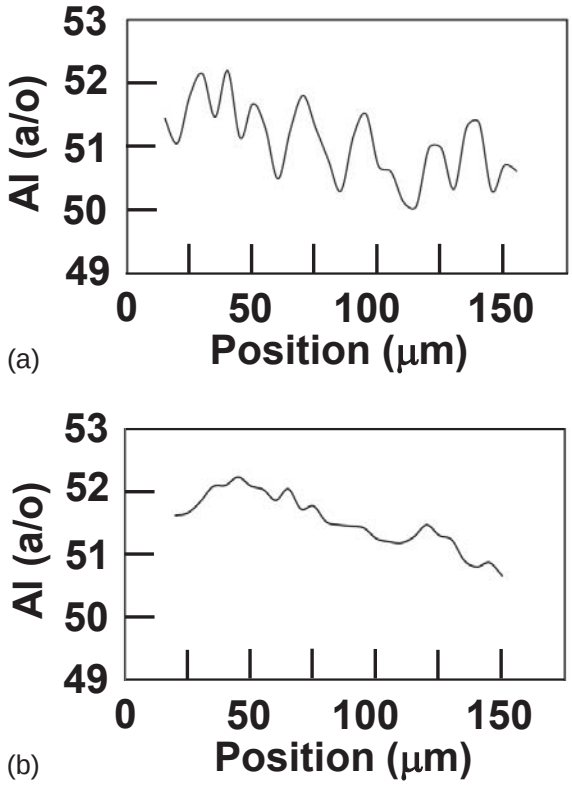

Figure 15. Aluminum composition profiles taken across EBPVD foil samples of Ti-51Al-1V (atomic percent) in (a) the as-fabricated condition or (b) following a subsequent 2 h heat treatment at 1423K (1150°C).

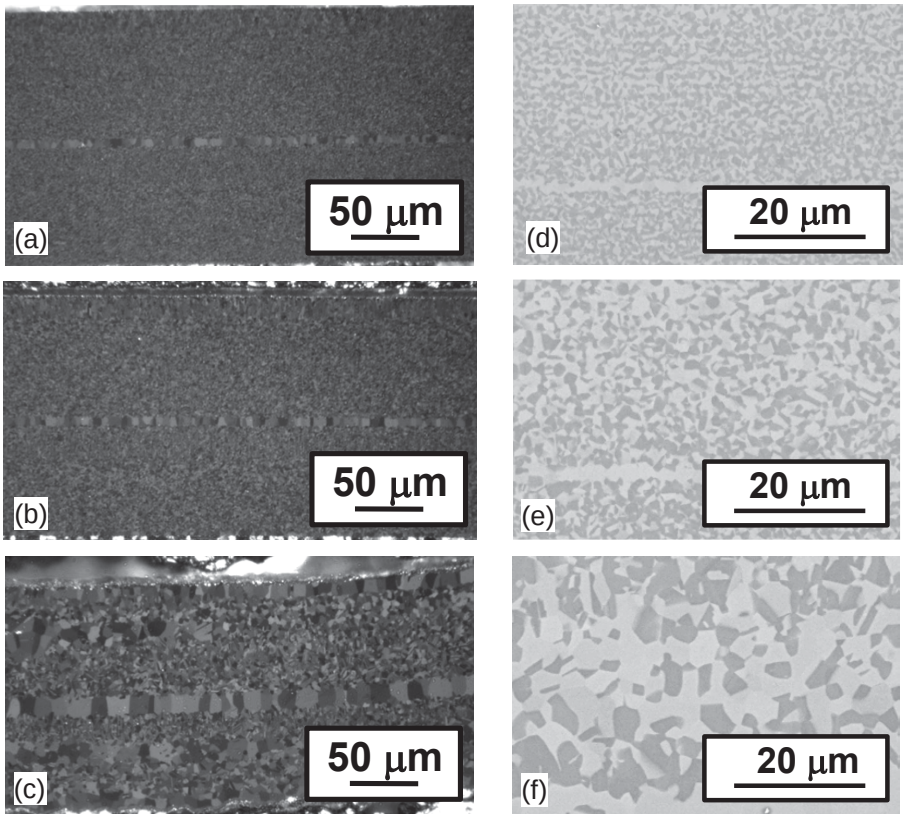

Figure 16. Microstructures in EBPVD foil of Ti-43Al (atomic percent) in (a, d) the as-deposited condition or following a following a 2 h heat treatment at (b, e) 1273K (1000°C) or (c, f) 1423K (1150°C); (a, b, c) polarized light, optical-microscopy images or (d, e, f) backscatter-electron images.